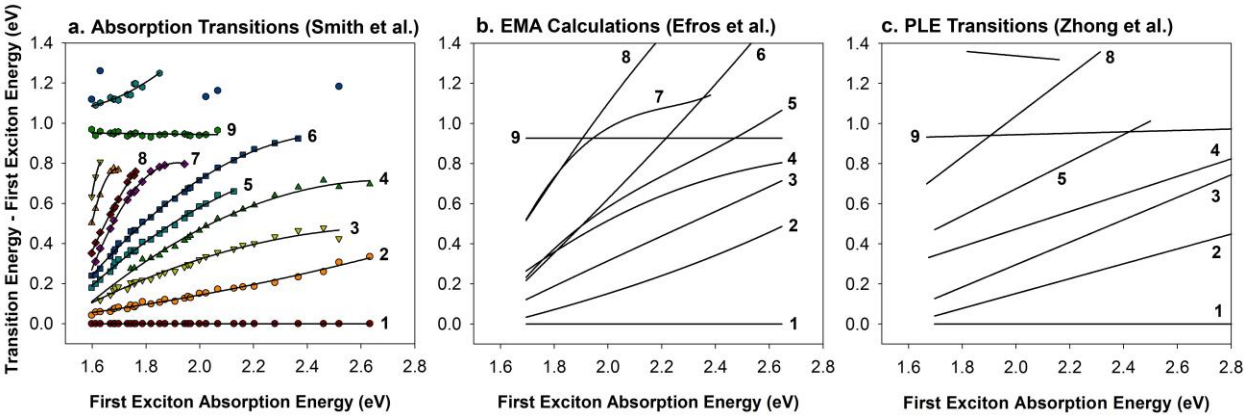

Supplementary Figure 1. Spectral analysis of CdTe nanocrystals with sizes between 2-12 nm diameter. (a) Absorption transitions were extracted from the 2nd or 4th derivative of the absorption spectra and plotted relative to the energy of the 1st exciton 1S(h)→1S(e) transition. Black lines are fittings of the transition trends, and transition notations correspond to assignments from effective mass approximations in (b). (b) Theoretical transitions 1-8 are derived from the effective mass approximation by Rosen and Efros for interacting bands, neglecting Coulombic and polarization contributions, and the split-off energy transition[1] (Transition 9 was assigned by Zhong et al.[2]). (c) Electronic transitions from CdTe nanocrystals derived from low-temperature photoluminescence excitation spectroscopy by Zhong et al.[2]

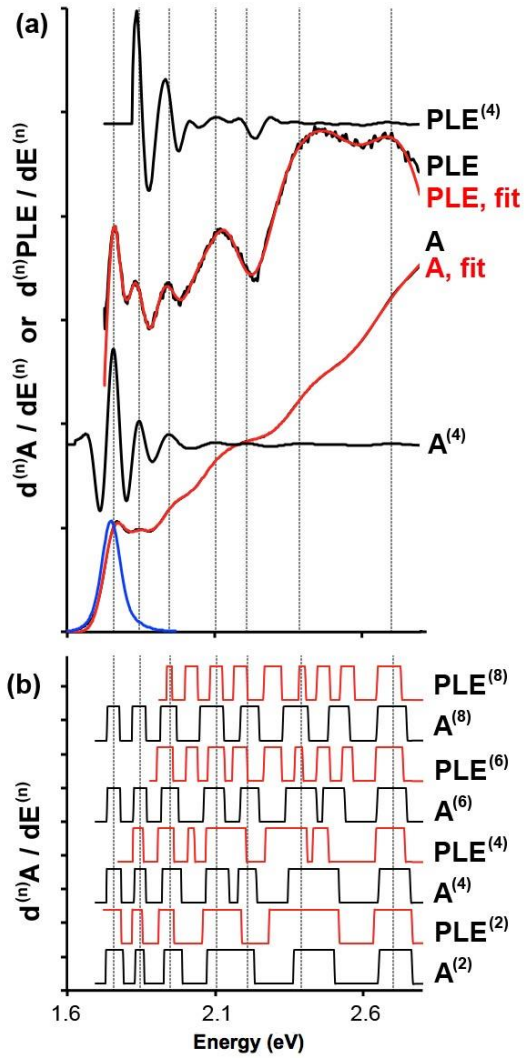

Supplementary Figure 2. Photoluminescence excitation (PLE) spectroscopy comparison with absorption spectroscopy for a 6.7 nm CdTe nanocrystal. (a) The collected absorption spectrum, A (black), is shown with its least square fit (red). The collected PLE spectrum is also shown in black with its least squares fit in red. The fluorescence spectrum is shown in blue. 4^{th} derivatives are shown for both the absorption and PLE spectra. (b) Flattened even-order derivative spectra are shown for both the absorption and PLE spectra. While substantially narrowed peak widths are obtained for PLE spectra, they do not reveal new transitions in the 0^{th} or 2^{nd} order spectra. Higher order derivatives of the PLE spectrum did reveal new transitions at energies higher than the 3^{rd} excitonic transition. The noise of PLE spectroscopy is substantially greater than that of absorption spectroscopy (especially for low quantum yield samples), which may contribute artifact peaks.

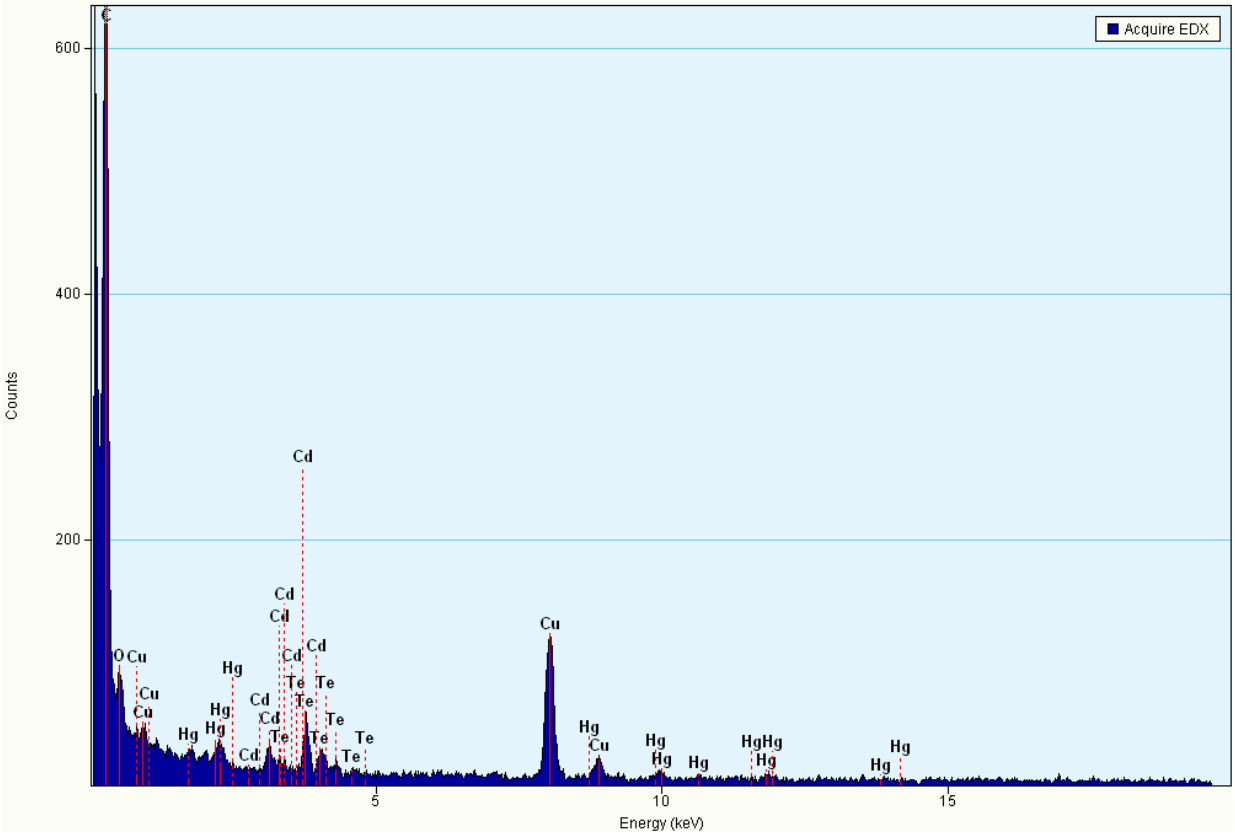

Supplementary Figure 3. Energy dispersive X-ray spectrum of 6.7 nm $Hg_xCd_{1-x}Te$ nanocrystals with x=0.30.

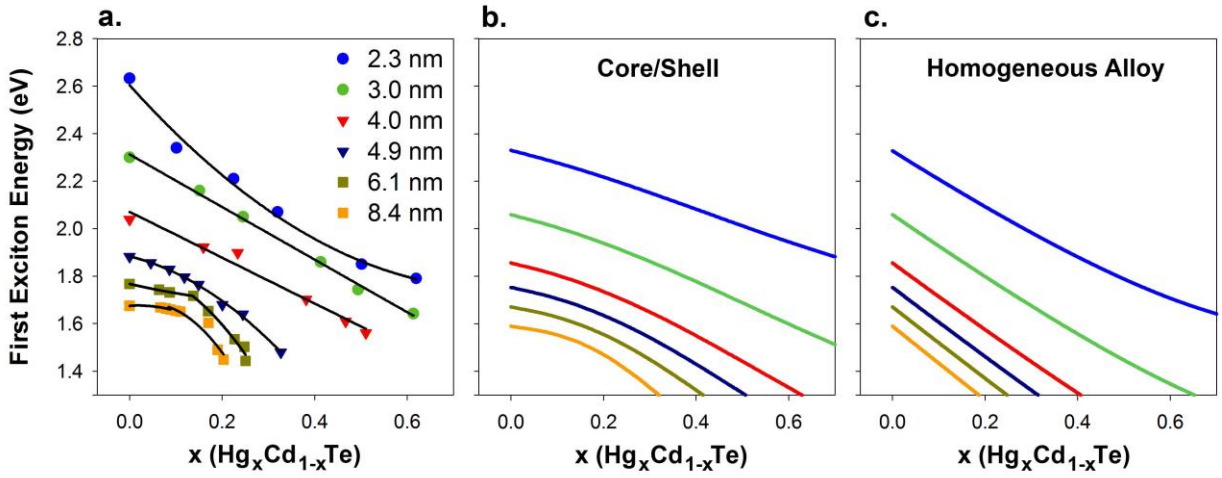

Supplementary Figure 4. First exciton energy of $Hg_xCd_{1-x}Te$ nanocrystals prepared through mercury cation exchange of CdTe QDs. (a) Correlation between total mercury content determined through ICP-MS and 1st exciton peak energy. (b) EMA calculations of $Hg_xCd_{1-x}Te$ nanocrystals with a core/shell CdTe/HgTe structure. (c) EMA calculations of $Hg_xCd_{1-x}Te$ nanocrystals with a homogeneous alloy structure. EMA calculations are for finite potential wells with Coulombic interactions added as a perturbation.

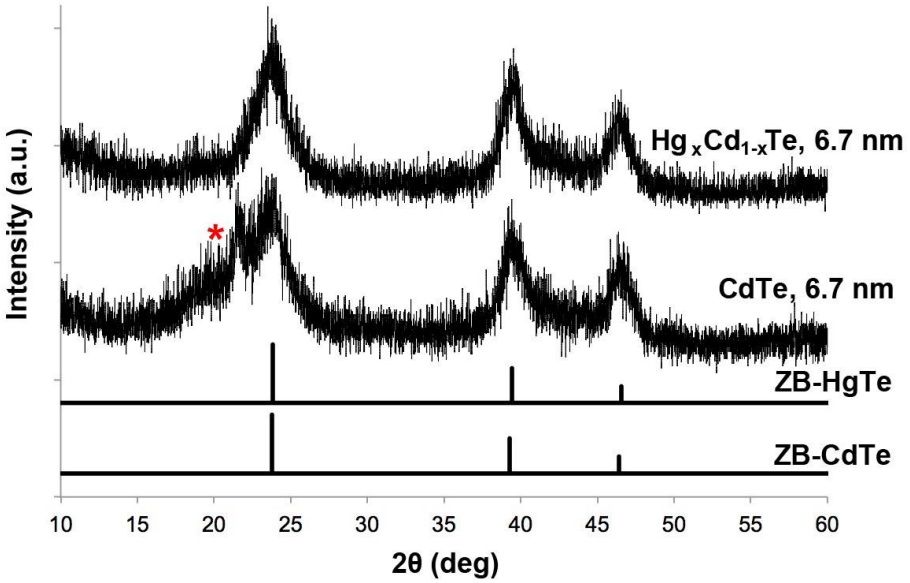

Supplementary Figure 5. Powder X-ray diffraction of 6.7 nm CdTe nanocrystals before and after cation exchange, showing retained crystallinity and lack of diffraction angle shift, in accord with the similar lattice parameters of zinc blende (ZB) CdTe and HgTe, shown below the diffraction data. The nearly identical domain sizes are reflected in the similar peak widths for the binary and ternary nanocrystals. Here x=0.30. The red asterisk indicates a scattering impurity (background was not subtracted).

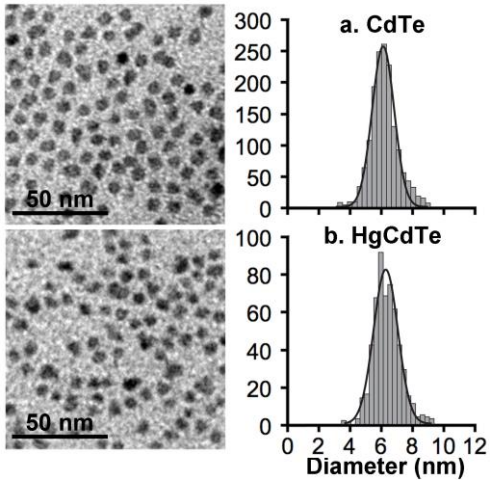

Supplementary Figure 6. Nanocrystal diameter does not significantly change during cation exchange, as determined from transmission electron micrographs and histograms of the sizes. (a) Before cation exchange: 6.12 ± 0.69; (b) after cation exchange: 6.24 ± 0.77.

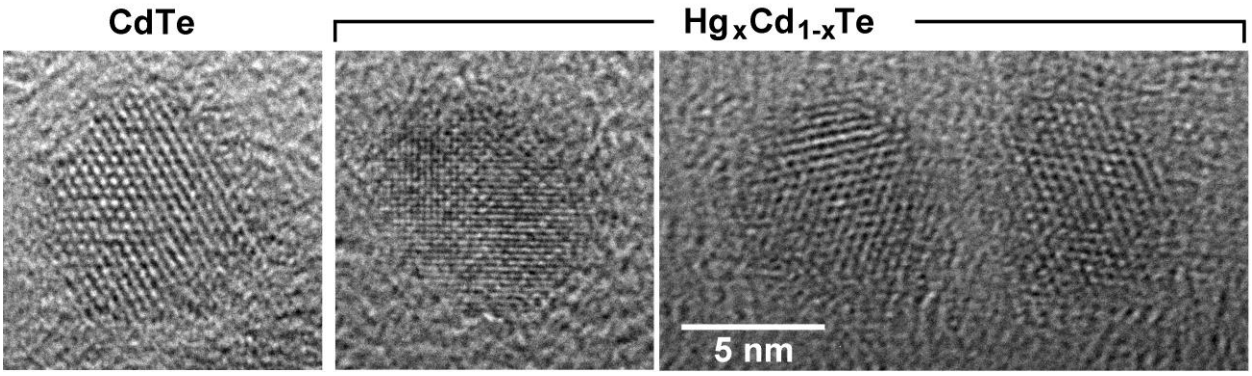

Supplementary Figure 7. High-resolution transmission electron micrographs of 6.7 nm CdTe nanocrystals before and after cation exchange, showing retention of crystallinity. Here x=0.30.

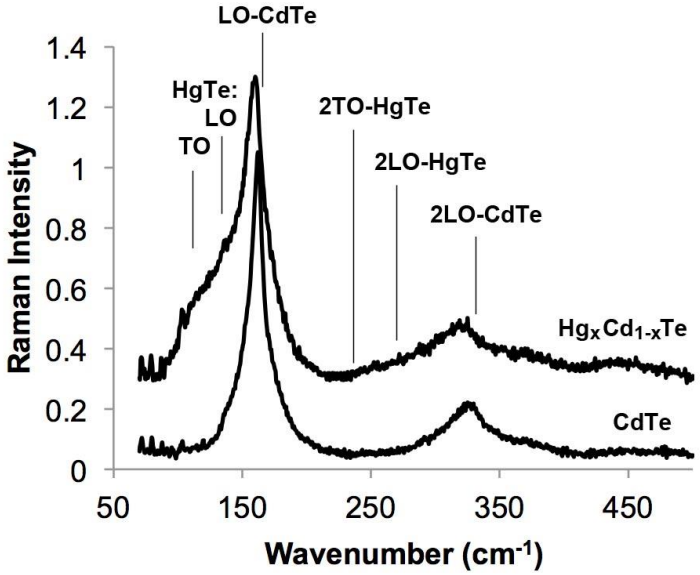

Supplementary Figure 8. Raman spectra of 6.7 nm CdTe nanocrystals before and after cation exchange. The LO and 2LO transitions are retained and broadened after cation exchange, reflecting a decrease in crystal domain size and lack of significant alloying. The new broad bands to at lower wavenumbers to LO-CdTe phonon modes can be assigned to HgTe modes, in accord with previous studies of $Hg_xCd_{1-x}Se$ materials,[3] with wide bands due to the small domain size. The 2TO and 2LO HgTe modes are very weak but contribute to a broad base not observed in the CdTe nanocrystal.

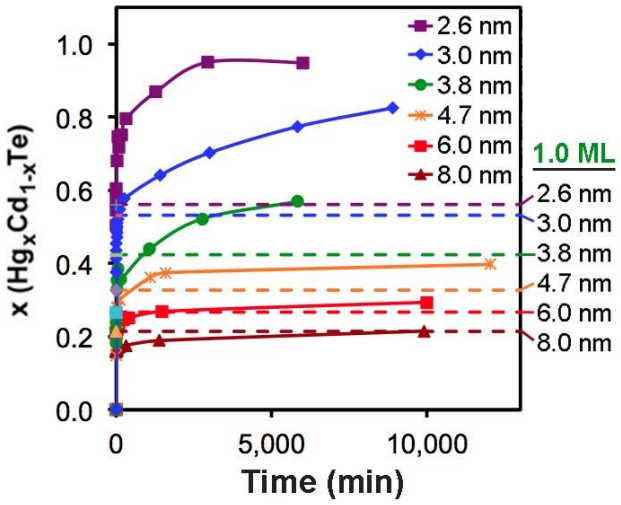

Supplementary Figure 9. Kinetic experiments of CdTe nanocrystal exchange with mercury octanethiolate. Nanocrystal composition was determined through absorption spectrophotometry and Equation 2 at different times after mixing with an excess of mercury (3-fold by total amount of Cd in the nanocrystals). Exchange occurred rapidly for all nanocrystals within the first few minutes, but leveled off to different values depending on the nanocrystal size. For the larger nanocrystals, this corresponded to the amount of mercury in one monolayer of shell, whereas for smaller particles, exchange beyond a single monolayer occurred rapidly. Dotted lines indicate the expected value of x for $Hg_xCd_{1-x}Te$ after exactly 1 monolayer of mercury exchange.

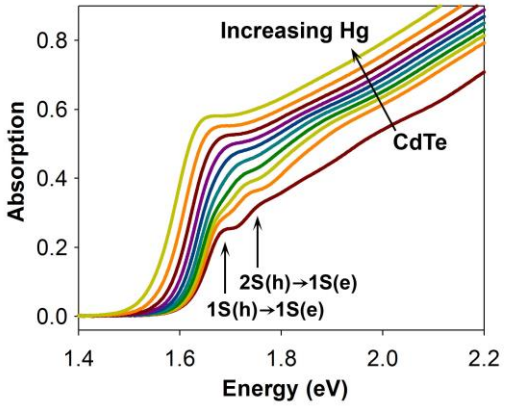

Supplementary Figure 10. Absorption spectra of 8.4 nm $Hg_xCd_{1-x}Te$ QDs, showing an increase in intensity of the 2nd exciton transition and other high energy transitions with increasing mercury content, and little change in the energy and intensity of the 1st exciton transition.

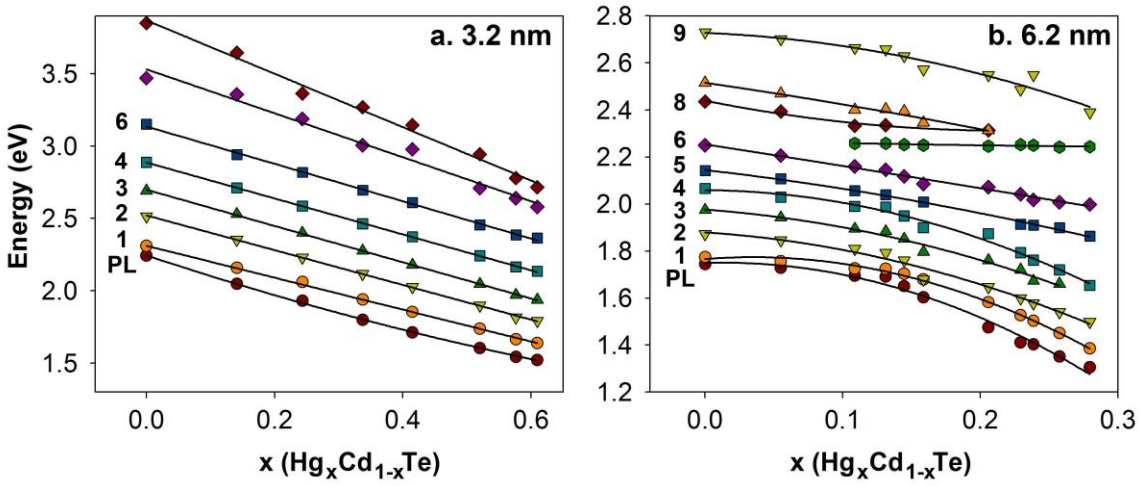

Supplementary Figure 11. Energy shifts in electronic transitions with composition for $Hg_xCd_{1-x}Te$ nanocrystals with a diameter of (a) 3.2 nm or (b) 6.2 nm. Transition assignments are denoted on the left side of the plot. PL is the photoluminescence peak transition. Transitions 1 and 2 are indistinguishable between x = ~0.14-0.19 for the 6.2 nm nanocrystal.

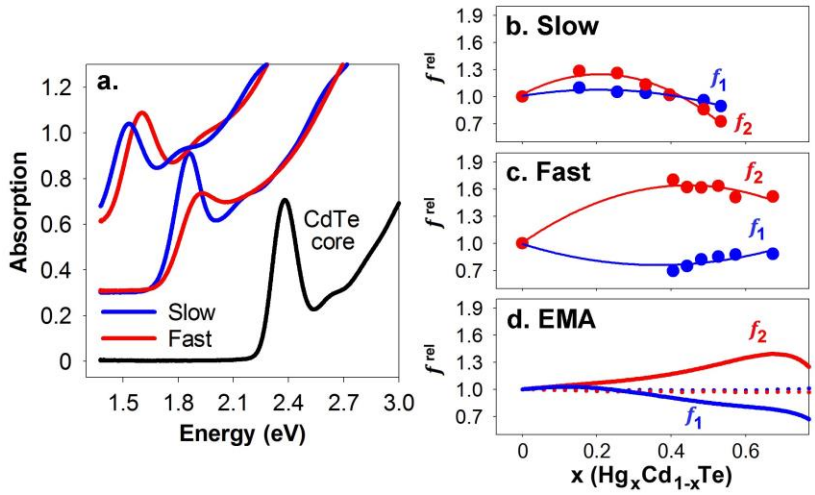

Supplementary Figure 12. Comparison between fast and slow methods for mercury cation exchange of small CdTe cores (3.2 nm). (a) Absorption spectra are shown for CdTe cores (black) and $Hg_xCd_{1-x}Te$ nanocrystals exchanged via slow exchange (blue) or fast exchange (red). Pairs of $Hg_xCd_{1-x}Te$ nanocrystal spectra with matching composition generated through either fast or slow exchange are plotted with the same offset for direct comparison. (b-d) Oscillator strengths for the 1st exciton transition (f_1, blue) and 2nd exciton transition (f_2, red) are shown: (b) slow exchange; (c) fast exchange; (d) EMA predictions for core/shell structure (solid lines) or homogeneous alloys (dashed lines).

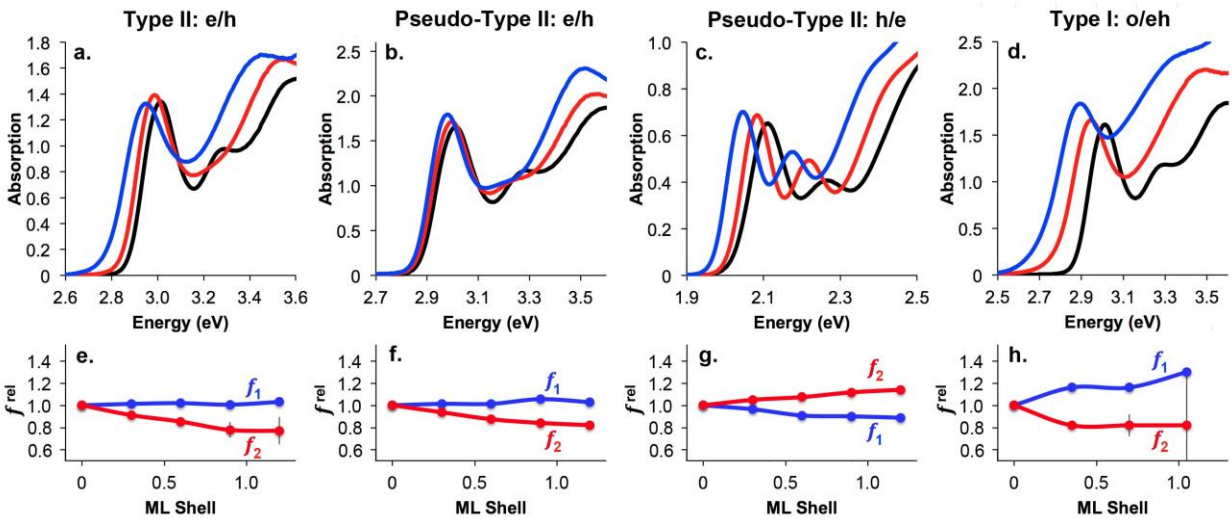

Supplementary Figure 13. Epitaxial shell growth in different carrier localization regimes. Absorption spectra are shown in a-d and relative oscillator strengths are plotted for the 1st exciton transition (f_1^{rel}) and 2nd exciton transition (f_2^{rel}) in e-g. Regimes are designated as: (a,e) Type II e/h (CdS/ZnSe), (b,f) Pseudo-Type II e/h (CdS/ZnS), (c,g) Pseudo-Type II h/e (CdSe/CdS), and (d,h) Type I o/eh with both the electron and hole in the shell (CdS/CdSe). Absorption spectra show cores with nominal shell thicknesses of 0 (black), 0.6 (red), and 1.2 (blue) monolayers (ML). Error bars are s.d.

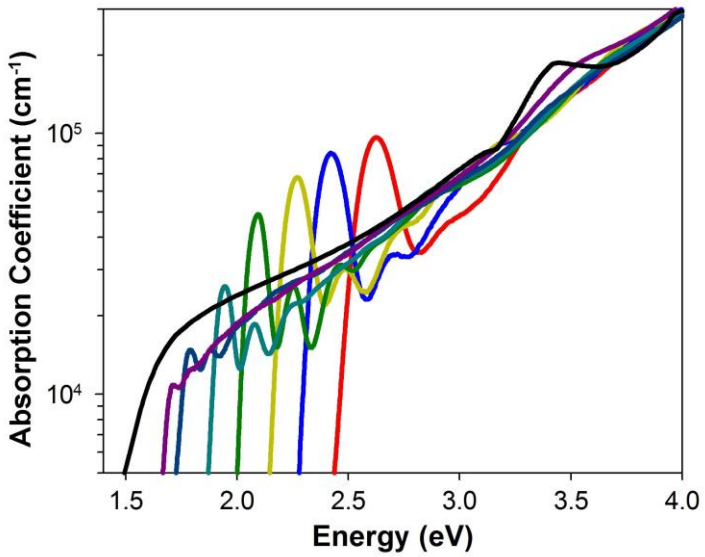

Supplementary Figure 14. Absorption coefficients of various sizes of CdTe nanocrystals, plotted with the bulk spectrum CdTe spectrum (black, extracted from Adachi et al.[4]) after adjusting for local field effects.

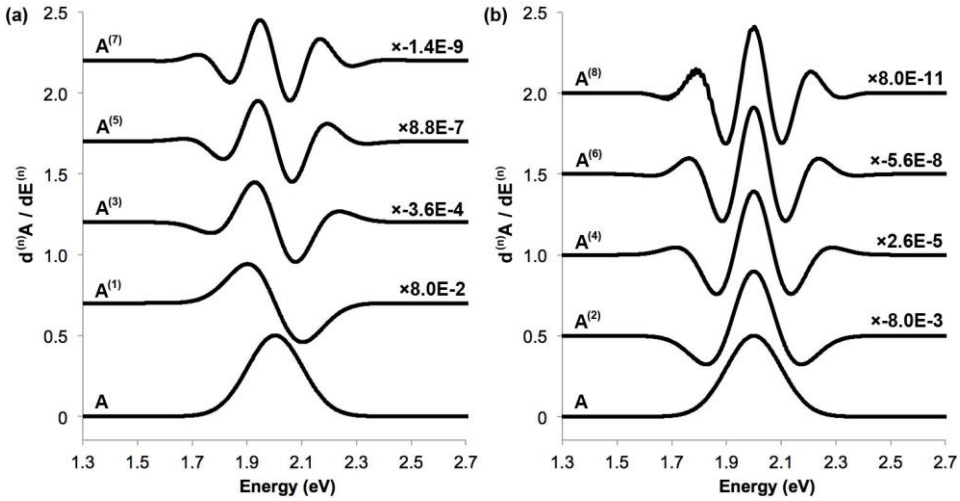

Supplementary Figure 15. Gaussian function A(E) and its (a) odd order derivatives and (b) even order derivatives. Functions are normalized by an intensity factor shown on the right of each plot. (n) = derivative order.

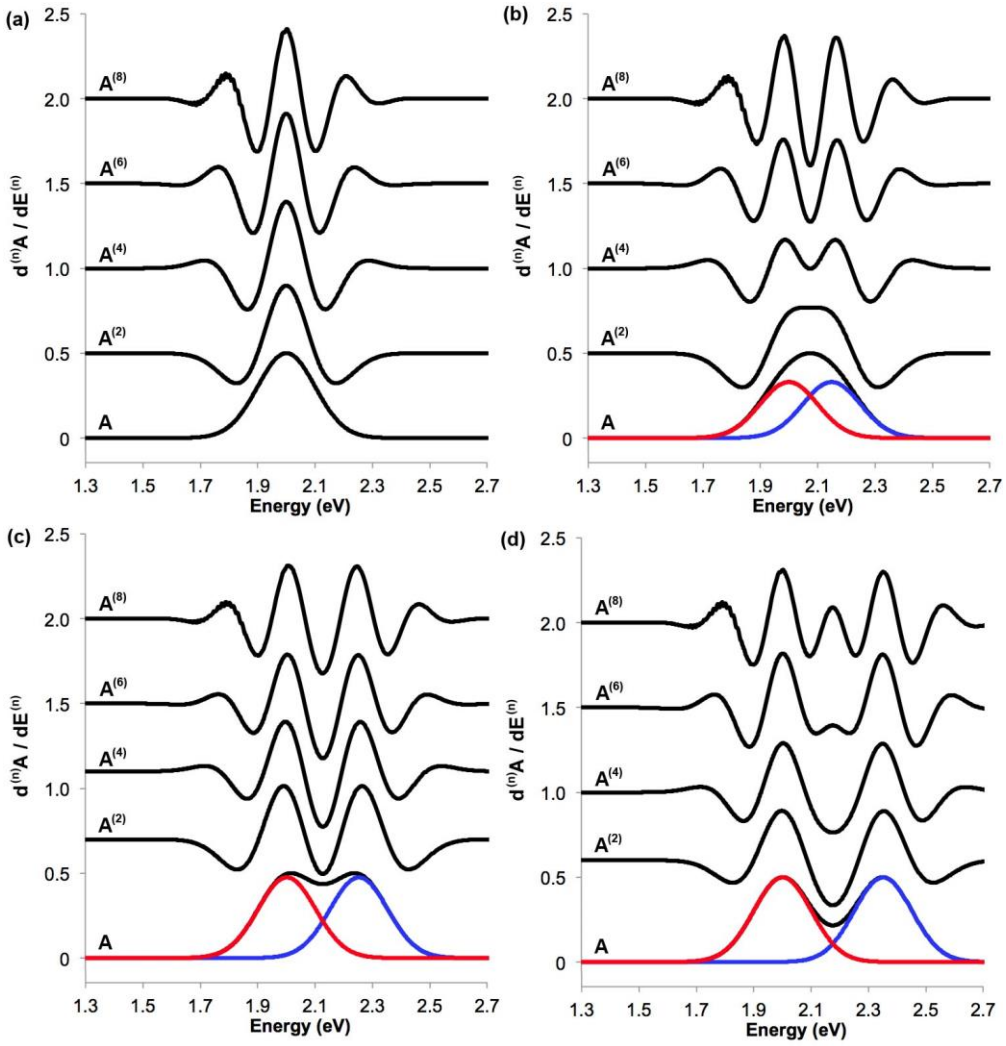

Supplementary Figure 16. Sums of two Gaussian functions (red and blue curves show the original input peaks and the black curve, A, is the sum). Four separation energies are shown: (a) 0 eV, (b) 0.15 eV, (c) 0.25 eV, or (d) 0.35 eV. The normalized even-order derivatives are shown above the original spectra.

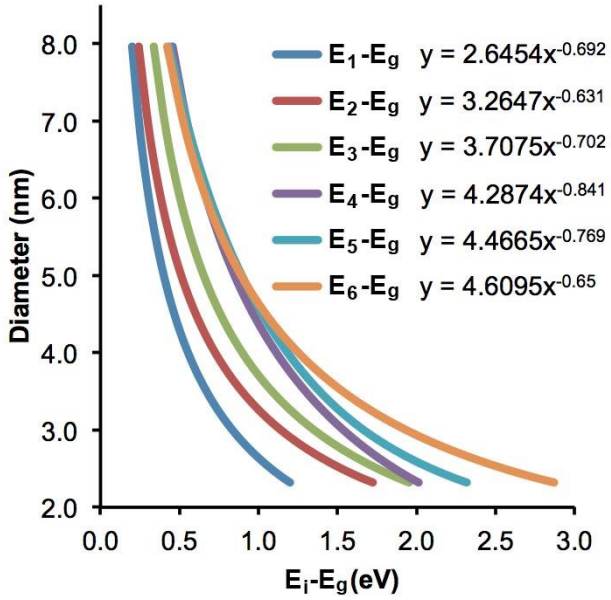

Supplementary Figure 17. Dependence of electronic transition energy on CdTe nanocrystal diameter, as calculated by Efros and Rosen.[1] Transitions are plotted as energy minus the bulk bandgap E_g.

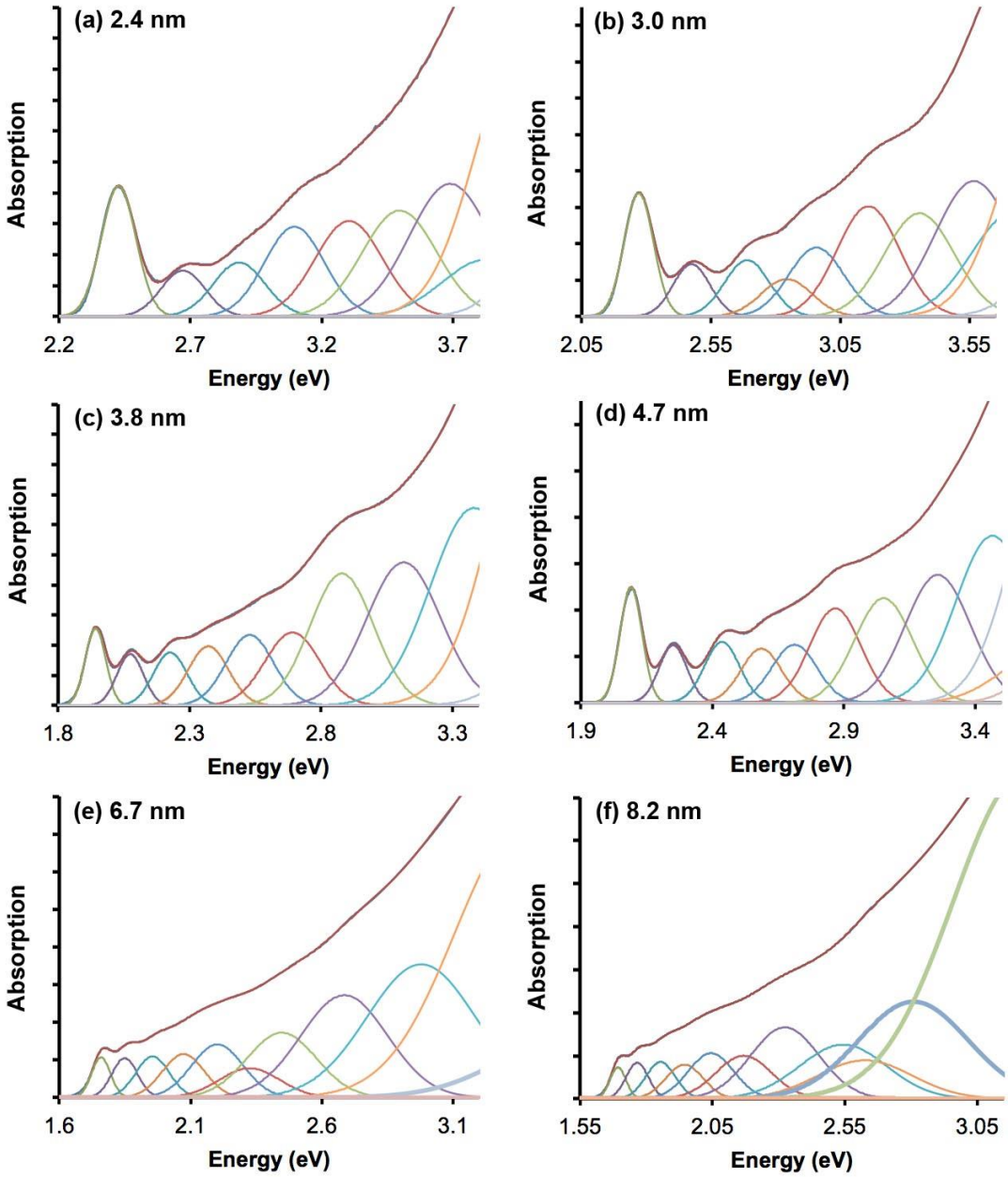

Supplementary Figure 18. Reconstruction of CdTe nanocrystal spectra for 6 different sizes. Original spectra are black and reconstructed curves are red. Multicolor Gaussians show the contributing transitions.

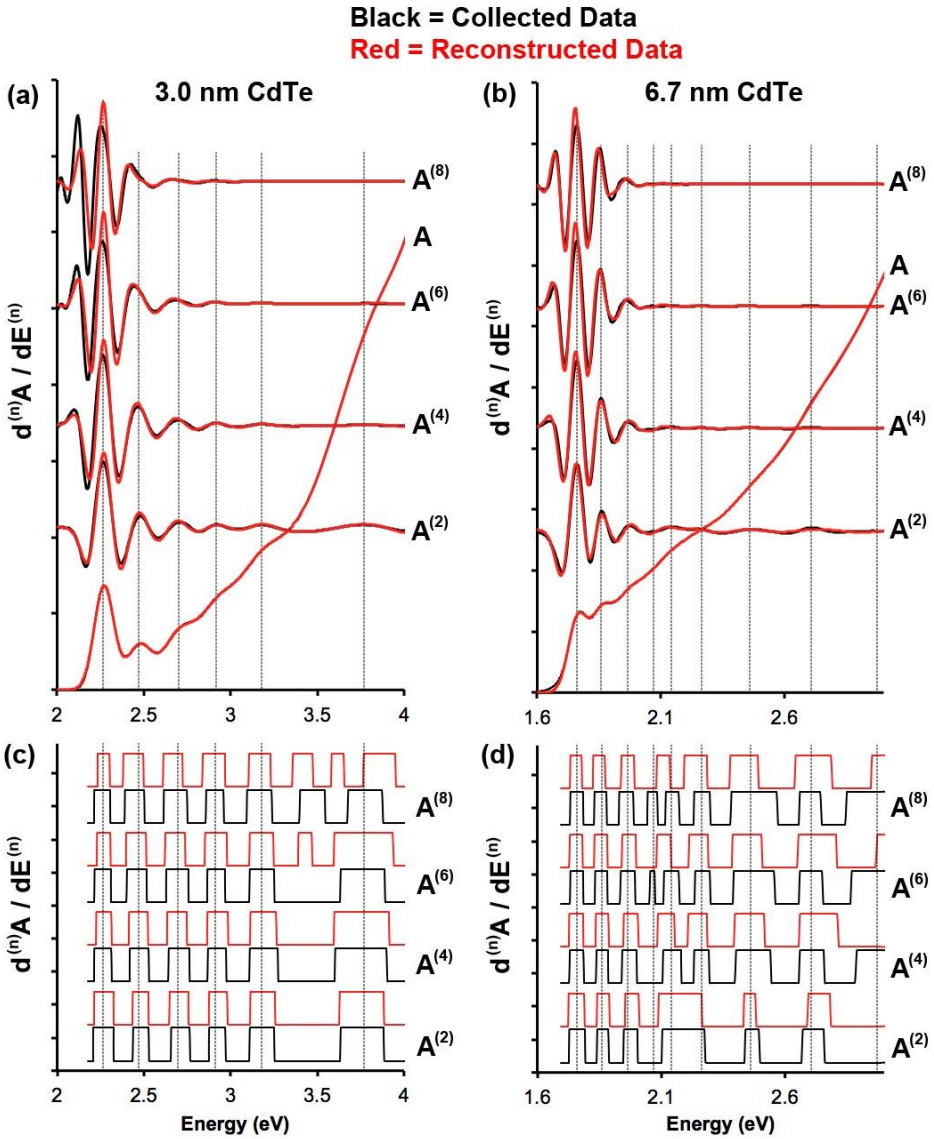

Supplementary Figure 19. Analysis of absorption spectra, A, of (a,c) 3.0 nm and (b,d) 6.7 nm CdTe nanocrystals, as well as their even-order derivatives, $A^{(n)}$. Experimentally collected spectra are shown in black and reconstructed spectra are shown in red. Extracted transition energies from the collected spectra are shown as dotted vertical lines. (c) and (d) show the even order derivatives after flattening to normalize intensity.

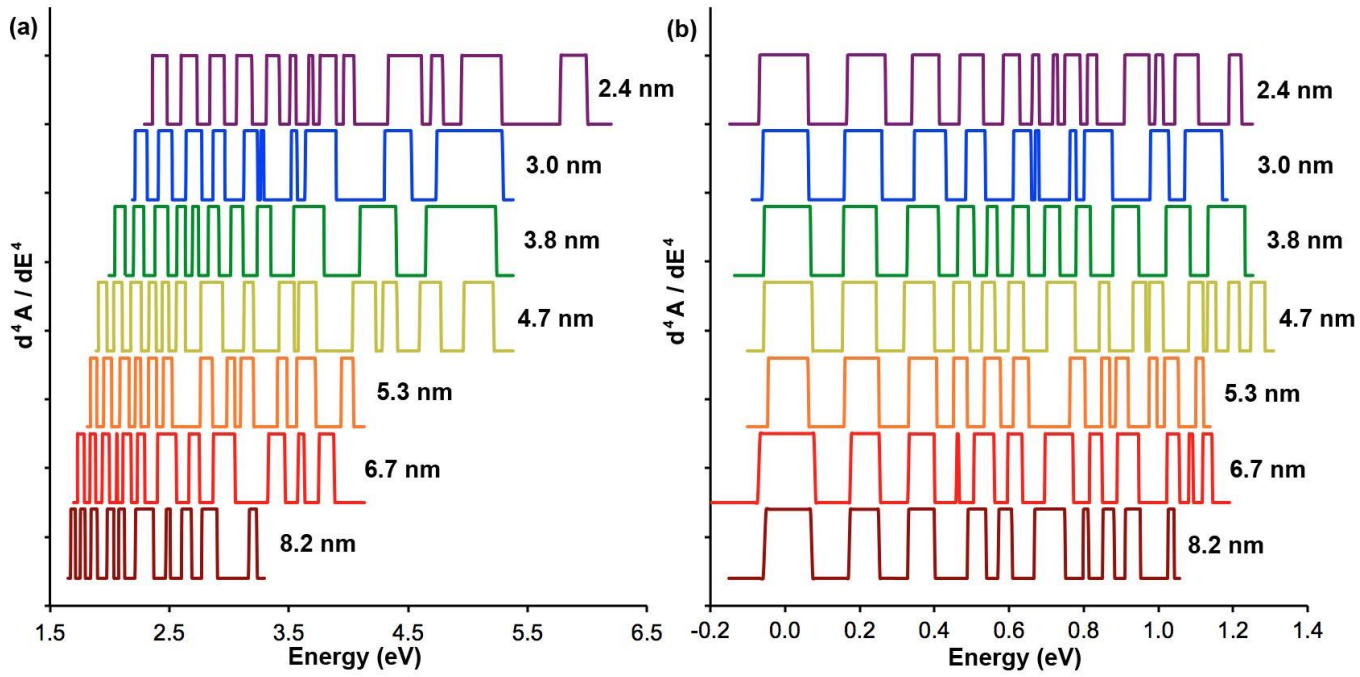

Supplementary Figure 20. (a) Flattened 4th derivative spectra of seven sizes of CdTe QDs. (b) Spectra are plotted with normalized by energy using the equation $E_{\mathrm{norm}} = \frac{E-E_1}{(E-E_{\mathrm{g}})^{0.714}}$.

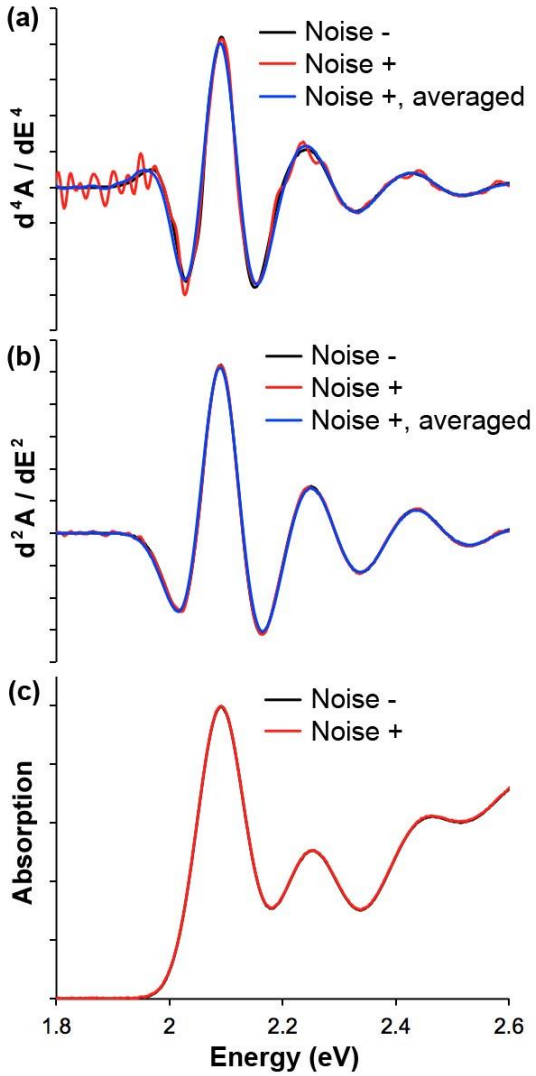

Supplementary Figure 21. The impact of noise on derivative spectra of CdTe nanocrystals. Shown are the original mathematically generated absorption spectrum with and without noise in panel (c), the 2nd derivative of each spectrum in panel (b), and the 4th derivative of each spectrum in panel (c). Blue curves in panels (b) and (c) show the averaged derivatives, which reproduce the noise-free spectra.

Supplementary Table 1. Parameters for Effective Mass Approximation Calculations

	m_e [5]	m_{HH} [5]	m_{LH} [5]	ε_∞ [5]	$E_g(\mathrm{eV})$ [5]	$\Delta E_V(\mathrm{eV})$ [6]	$\Delta E_C(\mathrm{eV})$ [6]	$a_{ZB}(\text{Å})$ [5]
ZnS	0.20	1.42	0.36	5.1	3.70	0	0	5.409
ZnSe	0.137	0.82	0.154	5.9	2.82	0.53	-0.35	5.668
ZnTe	0.117	0.67	0.159	6.9	2.39	1.26	-0.05	6.089
CdS	0.140	0.68	0.15	5.4	2.50	0.18	-1.02	5.818
CdSe	0.119	0.57	0.11	6.2	1.76	0.60	-1.34	6.052
CdTe	0.090	0.82	0.145	7.1	1.50	1.17	-1.03	6.482
HgTe	0.028	0.03	0.38	7.0	-0.15	1.53	-2.32	6.462
Solv.	1	1	1	1.375	7.8	-2.52	2.68	N.A.

ΔE_V and ΔE_C are the band offsets of the valence and conduction bands, respectively. a_{ZB} is the zinc blende lattice constant.

Supplementary Table 2. Optical transitions in CdTe QDs and $Hg_xCd_{1-x}Te$ nanocrystals

Transition Number	Transition Assignment*
1	$1S_{3/2}(h) \rightarrow 1S(e)$
2	$2S_{3/2}(h) \rightarrow 1S(e)$
3	$1P_{3/2}(h) \rightarrow 1P(e)$
4	$1S_{1/2}(h) \rightarrow 1S(e)$
5	$1P_{1/2}(h) \rightarrow 1P(e)$
6	$2P_{3/2}(h) \rightarrow 1P(e)$
7	$2S_{1/2}(h) \rightarrow 1S(e)$
8	$2P_{1/2}(h) \rightarrow 1P(e)$
9	$1S_{SO}(h) \rightarrow 1S(e)$

*Subscript notations for total angular momentum are omitted in the text for brevity.

Supplementary Methods

Determination of Transition Energies. Energies of electronic absorption transitions were determined through differential absorption spectroscopy (DAS). DAS is a commonly used technique for the analysis of UV-Vis spectra (including those of semiconductor nanocrystals[7-9]), IR spectra, and electron spin resonance spectra,[10,11] because even-order derivatives reduce widths of convolved bands to reveal low-intensity peaks and peaks that are too closely spaced to resolve in the original zero-order spectrum.[12] Electronic absorption spectra are typically modeled as sums of discrete transitions spread as Gaussian or Lorentzian functions (or a mixture of the two) with linewidths that are homogeneously and/or inhomogeneously broadened. The main contribution to broadening for colloidal semiconductor nanocrystals is the dispersion in nanocrystal size across an ensemble of particles, for which Gaussian curves provide strong fits,[13] with the exception of 2D platelet and quantum well structures which exhibit very little dispersion in the length dimension of confinement.[14] **Supplementary Figure 15** depicts a 2 eV Gaussian function, A(E), with a full-width-at-half-maximum (FWHM) of 0.235 eV, in addition to the first 8 derivatives with respect to energy, normalized in intensity by the factor on the right side of each function. Odd-order derivatives, $A^{(1)}$, $A^{(3)}$, $A^{(5)}$, and $A^{(7)}$, are plotted in (a) and even-order derivatives, $A^{(2)}$, $A^{(4)}$, $A^{(6)}$, and $A^{(8)}$, are plotted in (b). For odd derivatives, a point of zero intensity overlaps with the maximum of A. For even derivatives a point of maximum intensity occurs at the same energy as the Gaussian maximum, and the peak width decreases with increasing derivative order. This narrowing allows discrete transitions to be extracted from overlapping functions. It is important to note that $A^{(2)}$ only has maxima where there are Gaussian maxima, whereas higher order even derivatives show satellite maxima that increase in relative intensity and total number with increasing derivative order.[12]

Supplementary Figure 16 depicts even-order derivatives of the sum of two Gaussian functions of equal intensity (0.5) and FWHM (0.235 eV) (one is blue, one is red, sum is black) with different degrees of overlap. For strongly overlapping functions in **Supplementary Figure 16b**, multiple peaks are not discernable in A(E) but the derivatives clearly show contributions from two peaks, with energies similar to those of the two original peaks. The transitions become sharper with increasing derivative order. Peaks can be resolved that are separated by 0.63 half-widths for the 2nd derivative and 0.53 half-widths for the 4th derivative.[12] However, artificial peaks arise in high order derivatives when the peaks become very well separated, shown as the formation of a new peak between the two peaks in **Supplementary Figure 16d** for $A^{(6)}$ and $A^{(8)}$. In general, a combination of the 2nd and 4th derivatives is optimal for determining energy and number of peaks:[12] $A^{(2)}$ is useful for detecting convolved peaks without introducing "false positives," whereas higher order derivatives are useful to improve resolution in instances when more peaks are expected based on theoretical models or trends in spectral changes.[12]

The absorption spectra of quantum dots are sums of many quantum confined electronic transitions that can have substantial peak overlap even for homogeneous samples. Peak intensities reflect transition oscillator strengths and peak widths are both a function of sample homogeneity and transition energy. Plotted in terms of energy, quantum dot transitions increase in bandwidth with energy due to the decreasing slope of the diameter-transition energy relationship (see plot for CdTe in **Supplementary Figure 17**), reflecting the curvature of the contributing bands. To a first approximation for any generic QD, the peak width can be modeled with a FWHM proportional to $E_i - E_g$, where E_i is the peak maximum. A more accurate value for CdTe nanocrystals is $(E_i - E_g)^{-0.714}$, based on fitting to an average of trends from the first 6 transitions from Efros and Rosen (**Supplementary Figure 17**).[1]

For this work, we are interested in accurately extracting the energies of the first two electronic absorption transitions, the 1st and 2nd exciton transitions. To determine under which conditions the peak energies can be accurately extracted form quantum dot spectra, we used an automated code to extract peaks from the 4th derivatives of CdTe nanocrystals with 6 different diameters (2.4-8.2 nm diameter). Up to 15 potential transition peaks were extracted. Using these energies, the absorption spectra of the nanocrystals were reconstructed as Gaussian transitions using least squares curve fitting. **Supplementary Figure 18** shows the original spectra in black, curves fitted from Gaussian peaks in red, and individual contributing transitions in different colors. The reconstructed spectra fit the original spectra with a correlation coefficient better than 0.9999 in all cases. These spectra resemble the general absorption spectra of many direct-bandgap II-VI and III-V nanocrystals with homogeneous size distributions, including those of CdS, CdSe, InAs, and ZnSe, and the methods here should translate for the analysis of these materials.

We more closely analyzed the reconstructed spectrum fits for the 3.0 nm nanocrystals and 6.7 nm nanocrystals, as shown in **Supplementary Figure 19.** Panels (a) and (b) show the raw collected spectra in black and the reconstructed spectra in red. Dotted lines show transition energies that were extracted from the raw data using the 4th derivatives of the spectra. The even-order derivatives, $A^{(n)}$, for the collected and reconstructed spectra are also shown above the zero-order spectra. A strong match is found for all spectra and their derivatives, except for high order derivatives at energies below the bandgap (due to noise; see below). Because it is difficult to visually identify high energy transitions from derivative spectra due to large differences in intensity, it is useful to "flatten" the derivative spectra to obtain "digital" derivative spectra by raising each function to a small positive power (e.g. 0.0001). The flattened spectra are shown in panels (c) and (d) in **Supplementary Figure 19**. For both the 3.0 nm and 6.7 nm CdTe nanocrystals, the first three band-edge transitions were nearly identical for the collected data and reconstructed data. Small deviations between the collected and reconstructed data arise as higher energy transitions for higher derivative orders. Performing this type of analysis for multiple nanocrystal sizes or compositions is useful for tracking specific transition trends: for example, flattened spectra from multiple sizes of CdTe QDs are plotted in **Supplementary Figure 20a**, and shown with normalized in energy in **Supplementary Figure 20b**. However for the analyses performed for this manuscript, we strictly examined the unflattened spectra.

Spectral noise can have a significant impact on the derivative spectra, especially for higher order derivatives and transitions near the band edge. In **Figure 19a-b** the deviations between collected and reconstructed data of the 6th and 8th derivatives of spectra at energies lower than the band edge transition arise from low-level noise. To examine this further, we generated CdTe nanocrystal spectra with a 1st exciton peak absorption intensity of 1 and introduced white noise with intensity equal to the zero-absorption noise of our spectrophotometer (average of 0.0020). **Supplementary Figure 21** shows the original spectrum without noise (black) and with noise (red) as well as the 2nd and 4th derivatives. This level of noise has a very small impact on the 2nd derivative but has a more significant impact on the 4th. Even higher derivative orders show a greater impact from noise (not shown). This contribution can be eliminated by either smoothing the original spectrum prior to taking derivatives or by averaging the derivative over a larger number of values.[11] We use the latter method, which we find leads to accurate reproduction of the noise-free spectrum (see blue curves in **Figure 20a-b**).

Supplementary Discussion

It is important to note that despite a washed out appearance, a spectrum of overlapping transitions can still contain sufficient information to accurately decompose the spectrum into its constituent transitions. The eye is sensitive to changes in spectral curve intensity, but it is poorly sensitive to changes in spectral curvature (that is, the second derivative). But mathematically, second order changes in intensity are readily obtained and are necessary and sufficient information for spectral deconvolution. As can be seen in **Supplementary Figure 16b**, a spectrum that is a convolution of two Gaussians close in energy appears to the eye to be a single smooth Gaussian. However the curvature of this peak still indicates that the spectrum is a sum of two Gaussians, which becomes evident with increasing order of even-order derivatives. This is mathematically identical to the use of gradient and Laplacian filters in image processing to extract image information that is simply not apparent to the eye, a very common practice for the detection of edges in images.

The limits of applicability of this procedure obviously must be finite. With increasing transition bandwidth, at some point peaks will lose sharpness to such a degree that it is no longer possible to accurately extract transitions through derivatives. We have quantitatively determined these limits for quantum dot-like spectra, as shown in **Figure 3**. What may be surprising from these results is that the accuracy of peak extraction is still high even after the spectrum becomes nearly featureless to the eye. The accuracy depends on the instrument noise level (which is very low for absorption spectrophotometry) and signal level (here usually high, depending on sample concentration), as well as the degree of peak broadening/overlap. Our model accounts for all of these contributions using parameters obtained directly from our experimental spectra and yield reconstructed spectra with strong similarity to experimental spectra (**Supplementary Figure 19**). This assessment tells us that we can accurately determine the extracted peak energies for the 1^{st} and 2^{nd} exciton peaks (of utmost importance in this work) with 99% accuracy for quantum dots with spectra broadened by effective size dispersions corresponding to a 15% standard deviation in diameter. This is where we set our threshold for analyses in this paper. Notably, in the spectra shown in **Figure 3a-b**, a 15% dispersion in size corresponds to spectra that visually appear fairly featureless.

Interestingly, accurate extraction of peak position is not actually a necessity, but rather the correct number of peaks within a spectral window is the key necessity to accurately determine oscillator strength. As long as we are not missing a present peak (underfitting) or artificially introducing a peak (overfitting), an accurate fitting algorithm will minimize the spectral deviations to maximize the fit to the original curve as long as the peak positions are unbounded within a sufficiently broad position range. Indeed even the best PLE spectra that are exceptionally sharp do not reveal the true peak centroids, as they still overlap with shoulders of adjacent peaks, which shift the centroid to a degree that depends on separation distance. A fitting algorithm would move the observed centroids to reveal the true positions. We are highly confident in the number of peaks within a spectral window because of the following 3 pieces of evidence.

(i) We have analyzed widely separated, discrete spectra of small CdTe nanocrystals that have very sharp transitions visible to the eye, corresponding to 7% standard deviation in diameter. Our derivative spectroscopy technique yields peaks that visually match the narrow spectra. This qualitative analysis is corroborated by PLE studies that further narrow spectra (our own and those in the literature). Importantly, no new peaks were detected in our CdTe PLE spectra (or in those of the literature) for at least the first 4 lowest energy electronic transitions for all sizes of nanoparticles.

(ii) We track transitions as incremental changes in energy/position with incremental changes in nanocrystal size or composition. Incremental tracking allows us to definitively assign peaks that have shifted to ensure the accurate numbers of peaks are still present.

(iii) The peak energies that we extracted strongly correspond with theoretical predictions (see **Supplementary Figure 1**).

Regarding higher order derivatives, we have used an automated code to extract peaks using the 4^{th} derivatives and the peak energies. The 4^{th} derivative was not the only possible approach, but we validated this choice by overlaying the spectra together with the 2^{nd}, 4^{th}, 6^{th}, and 8^{th} derivatives, in addition the reconstructed spectra with their same derivatives, as is demonstrated in **Supplementary Figure 19a-b**. This allowed us to visually determine which derivative order most strongly corresponded with true peaks in reconstructed spectra. Thus this analysis did not simply require the 4^{th} derivative – the 2^{nd} derivative worked very well but overall we found that the 4^{th} derivative was the optimum balance of sensitivity to minor peaks while preventing over-extraction of artificial peaks observed in the 8^{th} derivative at high energies. Extraneous peaks only arise where noise was very large compared with signal, occurring only at energies much smaller than the band edge. Notably, the 4^{th} derivative and other higher order peaks are used commonly in applied spectroscopy, as referenced in **Supporting Methods**.

Concerning peak "flattening," it is important to point out that this procedure was not used in any of the spectral analysis performed in this paper, but was contrived as a convenient visualization tool for this manuscript after all of the analysis was performed. In practice, we expanded and contracted the y-intensities for evaluation of the peaks. We believe that the flattening procedure is very useful for comparing different peaks, and we intend to use this in the future, as we found that zero noise peaks were amplified at energies greater than that of the first exciton. This is the result of the high signal-to-noise ratio of absorption spectrophotometry.

Regarding the EMA theoretical model employed in this paper, our major goal was to employ a method that can be widely employed for the assessment of nano-heterostructures. The modeling accuracy could be further improved through more complex calculations that include additional terms accounting for band non-parabolicity, band mixing, surface states, etc., but these types of analysis methodologies could not be readily implemented by those lacking extensive training in computational methods and modeling or individuals who do not have access to computational power needed to solve such problems in a reasonable amount of time. We believe that there is great value in obtaining reasonable results with a much simpler method that can readily be visualized, interpreted, and applied. The major contribution to the effects that we observe is expected to be the quantum confinement effect, which is the same underlying principle in the more complex and simpler models. This is in accord with the correlation of major trends between theory and experiment observed in our work, as well as a large body of previous work. An analogous situation is that there are widespread molecular dynamics simulation programs which can offer more accurate diffusion coefficients for particle motion in a Newtonian medium, but the classic Stokes-Einstein equation introduced in 1905 is still heavily used to give values sensibly close to experimentally observed values using parameters and results that can be grasped by most non-experts as an aid for developing intuition and insight.

In addition, it is important to note that the EMA model that we applied does not require an ad-hoc addition of an exponential term to break orthogonality between the electron 1s and hole 2s wavefunctions. This is because the electron and hole experience different potential offsets between the nanocrystal and matrix and have different effective masses, and thus exhibit different levels of confinement and tunneling into the surroundings, causing the set of the

eigenfunctions between the electron and the hole to be non-equivalent. This creates a nonzero overlap between the electron 1s and hole 2s states, and thus nonzero oscillator strength. The addition of the exponential term provides greater accuracy for the 1s-2s overlap value, but is not required to obtain nonzero values. The easy interpretation of the results of this model highlight the great strength – the "simple" shift in 2^{nd} exciton peak oscillator strength is driven by small changes in the degree of tunneling into the surroundings mediated by a combination of carrier mass and potential offsets.

Supplementary References

1 Efros AL & Rosen M. Quantum size level structure of narrow-gap semiconductor nanocrystals: effect of band coupling. *Phys. Rev. B* **58**, 7120-7135 (1998).

2 Zhong H, Nagy M, Jones M & Scholes GD. Electronic states and exciton fine structure in colloidal CdTe nanocrystals. *J. Phys. Chem. C* **113**, 10465-10470 (2009).

3 Prudnikau A, Artemyev M, Molinari M, Troyon M, Sukhanova A, Nabiev I, Baranov AV, Cherevkov SA & Fedorov AV. Chemical substitution of Cd ions by Hg in CdSe nanorods and nanodots: spectroscopic and structural examination. *Mater. Sci. Eng. B* **177**, 744-749 (2012).

4 Adachi S, Kimura T & Suzuki N. Optical properties of CdTe - experimental and modeling. *J. Appl. Phys.* **74**, 3435-3441 (1993).

5 Adachi S. *Properties of Group-IV, III-V and II-VI Semiconductors* (John Wiley & Sons, 2005).

6 Wei SH & Zunger A. Predicted band-gap pressure coefficients of all diamond and zinc-blende semiconductors: Chemical trends. *Phys. Rev. B* **60**, 5404-5411 (1999).

7 Ellingson RJ, Beard MC, Johnson JC, Yu PR, Micic OI, Nozik AJ, Shabaev A & Efros AL. Highly efficient multiple exciton generation in colloidal PbSe and PbS quantum dots. *Nano Lett.* **5**, 865-871 (2005).

8 Vossmeyer T, Katsikas L, Giersig M, Popovic IG, Diesner K, Chemseddine A, Eychmuller A & Weller H. CdS nanoclusters: synthesis, characterization, size dependent oscillator strength, temperature shift of the excitonic transition energy, and reversible absorbance shift. *J. Phys. Chem.* **98**, 7665-7673 (1994).

9 Cademartiri L, Montanaro E, Calestani G, Migliori A, Guagliardi A & Ozin GA. Size-dependent extinction coefficients of PbS quantum dots. *J. Am. Chem. Soc.* **128**, 10337-10346 (2006).

10 Sanchez Rojas F, Bosch Ojeda C & Cano Pavon JM. Derivative ultraviolet-visible region absorption spectrophotmetry and its analytical applications. *Talanta* **35**, 753-761 (1988).

11 Antonov L & Nedeltcheva D. Resolution of overlapping UV-Vis absorption bands and quantitative analysis. *Chem. Soc. Rev.* **29**, 217-227 (2000).

12 Griffiths TR, King K, St. A. Hubbard HV, Schwing-Weill MJ & Meullemeestre J. Some aspects of the scope and limitations of derivative spectroscopy. *Anal. Chim. Acta* **143**, 163-176 (1982).

13 Klimov VI. Optical nonlinearities and ultrafast carrier dynamics in semiconductor nanocrystals. *J. Phys. Chem. B* **104**, 6112-6123 (2000).

14 Achtstein AW, Schliwa A, Prudnikau A, Hardzei M, Artemyev MV, Thomsen C & Woggon U. Electronic Structure and Exciton-Phonon Interaction in Two-Dimensional Colloidal CdSe Nanosheets. *Nano Lett.* **12**, 3151-3157 (2012).